Effect of Al₂O₃ Particle Size on Mechanical Properties of Al-12%Si Alloy via Taguchi Method

Farah Ammar Ibrahim[1]*, Zeyad D. Kadhim[1], Mohammed Abdulraoof Abdulrazzaq[1], Abdelhedi Aydi[2]

[1] Materials Engineering Department, College of Engineering, Mustansiriyah University, Baghdad 10054, Iraq
[2] Laboratory of Spectroscopic Characterization and Optical Materials, Faculty of Sciences, University of Sfax, Sfax 3026, Tunisia

Corresponding Author Email: farahammar@uomustansiriyah.edu.iq

ABSTRACT

This research investigates the impact of incorporating aluminum oxide (Al₂O₃) particles of varying sizes (25, 50, and 100 µm) into an Al-12%Si alloy to improve its mechanical and wear characteristics. A consistent weight fraction of 3% Al₂O₃ was utilized, and the composites were fabricated through stir casting. The evaluation of their hardness, wear rate, and microstructural features was conducted using standard methodologies, including Vickers hardness testing, pin-on-disc wear testing, and X-ray diffraction. To refine the testing parameters, the Taguchi method was employed, followed by ANOVA to assess the impact of significant factors such as particle size, load, and duration. Among the samples evaluated, the composite reinforced with 25 µm Al₂O₃ particles exhibited the most favorable performance, attaining a peak hardness of 102 HV (in contrast to 80 HV for the base alloy) and the lowest wear rate, reflecting a reduction of approximately 32%. These enhancements are primarily ascribed to the smaller particles facilitating improved dispersion, enhanced bonding, and more effective hindrance of dislocation movement. The results underscore the essential role of reinforcement size while also illustrating the benefits of statistical optimization in minimizing experimental workload.

1. INTRODUCTION

Aluminum metal matrix composites (AMCs) are unique materials that are made up of an aluminum matrix and a secondary part that makes it stronger. The second phase is generally a material that is more durable, strong, or less likely to break. These aluminium alloys are good for making AMCs because they are light, strong, and don't expand or contract much when heated or cooled. They can also be recovered, shaped easily for mass production, and withstand corrosion well. There are three kinds of composite materials. They are called Metal matrix composites (MMCs), Ceramic matrix composites (CMCs), and Polymer matrix composites (PMCs) [1, 2]. They can improve mechanical properties like hardness, Young's modulus, 0.2% yield strength, and final tensile strength the most because they contain nano and micro-sized reinforcement particles. This is because these are what they are made of. Cast aluminium alloys are used a lot in the car and aeroplane businesses all over the world. owing to their remarkable specific strength and stiffness, low density, and outstanding casting characteristics [3, 4].

The most frequently utilized metal matrices include aluminum, magnesium, titanium, and their respective alloys. The rationale for employing these materials lies in their reduced weight, affordability, and accessibility. Similarly, reinforcements are categorized into fibers, filaments, and particles [5]. Al₂O₃ particles, characterized by their elevated specific stiffness and exceptional high-temperature properties, serve as inert ceramic reinforcement phases in MMCs [6]. Metal matrix composites integrate hard ceramic particles within the matrix to enhance hardness, yield strength (YS), and ultimate tensile strength (UTS) [7].

Aluminum metal matrix composites are fortified with discontinuous reinforcements, which enhance their physical and mechanical properties [8]. Aluminum alloys are employed in engineering due to their ductility, resistance to corrosion, favorable strength-to-weight ratio, and affordability [9, 10]. Al-Si alloys can be categorized according to their silicon content into three types: hypoeutectic (containing less than 12 wt.% Si), hypereutectic (containing >12 wt.% Si), and eutectic (containing exactly 12 wt.% Si) [11]. Stir casting is broadly recognized for its cost-effective processing capabilities, enabling a higher production rate in the preparation of aluminum metal matrix composites (MMCs) through the reinforcement of various elements and other intricate products [12, 13].

Casting is a more economical method in comparison to different production techniques, with stir casting frequently recognized as a commercially proven method. Additionally, stir casting allows for the replacement and integration of traditional metal processing techniques, resulting in cost savings. Nevertheless, when utilizing the stir casting method for the fabrication of metal matrix composites, it is crucial to carefully evaluate various factors, including the difficulty of

ensuring proper allocation of reinforcement materials and the porosity present in the cast metal matrix composites [14]. In solid-state manufacturing, the adhesion between the matrix and reinforcing agents takes place as a result of the mutual diffusion that transpires between them under high-pressure and temperature conditions in the solid state [15].

Reinforcements are integrated into the molten matrix during the production phase in a liquid state, after which the matrix solidifies through casting or infiltration methods. In comparison to solid-state manufacturing methods, liquid-state techniques are generally more economical. Among the various liquid state methods, stir casting stands out as a commonly utilized and cost-efficient technique that enhances wettability, reduces porosity, and ensures a relatively uniform distribution of reinforcements within the matrix [15, 16].

This research explores the enhancement of aluminum silicon alloys using Al_2O_3 via a stir casting technique, analyzing how this additive influences the wear resistance, hardness, and microstructural properties of the aluminum silicon alloy.

2. EXPERIMENTAL WORK

2.1 Materials

Composite specimens were created utilizing Al and Si as the foundational metals, with Al_2O_3 acting as the ceramic reinforcement, through the stir casting technique. The chemical composition of the eutectic Al-Si alloy is outlined in Table 1. Al_2O_3 powder, which has a particle size of 25, 50, and 100 μm, was added to the molten Al-Si with the aid of a mechanical stirrer [17, 18].

2.2 Eutectic Al-Si composite specimen preparation

In this research, the process of fabricating the Al-Si composite commenced with the insertion of commercially pure aluminum wires into a clay-bonded graphite crucible. The crucible was subsequently heated in a gas-fired furnace under standard atmospheric conditions, without the use of inert gas shielding such as argon. Once the aluminum had completely melted, silicon was incrementally added and manually stirred with a graphite rod to ensure thorough dissolution and homogenization. After achieving a consistent Al–12 wt% Si alloy melt, alumina (Al_2O_3) particles—at a concentration of 3 wt% and with particle sizes of 25 μm, 50 μm, and 100 μm— were integrated into the melt. Mechanical stirring was performed at a regulated rotational speed of 630 rpm. The ceramic particles were gradually introduced into the vortex formed within the melt over a duration of less than five minutes, at a processing temperature of 750°C, to facilitate uniform dispersion [19]

This method is commonly employed in practice to improve the distribution of reinforcement particles within the matrix. Following this, approximately 1 gram of aluminum chloride ($AlCl_3$) solution was added to the melt to enhance the wettability between the ceramic particles and the metallic matrix. After a brief stirring period, slag residues were eliminated from the surface of the melt. Thereafter, the composite melt was poured into a preheated cast iron mold maintained at around 300°C. The preheating was designed to decrease the solidification rate and reduce the formation of porosity. The casting resulted in a cylindrical rod with dimensions of 14 mm in diameter and 22 cm in length. Ultimately, the as-cast composite underwent a homogenization heat treatment at 500°C, followed by gradual cooling in a furnace under ambient air conditions to refine the microstructure and ensure uniform grain distribution.

Table 1. Demonstrate the chemical composition of the Al-Si alloy

Elements	Al-Si Alloy
Si %	12.3
Fe %	0.27
Cu %	0.008
Mn %	0.002
Mg %	0.003
Cr %	0.004
Ni %	0.136
Zn %	0.014
Ti %	0.015
Pb %	0.001
Al %	Bal

2.3 SEM test

The alloy specimens were meticulously prepared for microstructural analysis by cutting them to a precise length of 20 mm. Each sample was subjected to grinding with emery papers of various grades (220, 400, 600, 800, 1000, 1200, 1500, and 2000). Water was utilized as a coolant to mitigate temperature increases. Subsequently, the specimens were polished with diamond paste and immersed in Keller's solution (which consists of 1 ml HF, 1.5 ml HCl, 2.5 ml HNO_3, and 95% water) for a period of 15 seconds. After this process, they were rinsed with alcohol and water, dried using hot air, and prepared for examination [20].

2.4 Hardness test

The Vickers hardness test was utilized in this research to evaluate the hardness of the samples. A load of 1 kg was exerted for a period of 15 seconds, following which the penetration diameter was calculated using the subsequent equation [21].

$$HV = 1.854 \times P / d(Av)^2 \tag{1}$$

In this equation, HV signifies the Vickers hardness, (P) where the symbol represents the load measured in kilograms, and d(Av) represents the mean length of the two diagonals formed by the indentation created by the indenter.

2.5 Wear test

In the present investigation, a pin-on-disc device was utilized for the assessment of wear. The specimens were fabricated with a length of 30 mm and a diameter of 10 mm. Three distinct loads 10 N, 15 N, and 20 N were exerted, accompanied by a sliding velocity of 340 m/s, across different time intervals of 10, 15, and 20 minutes.

The wear rate for the specimens was calculated using the subsequent equation [22].

$$\text{Wear Rate (W.R)} = \Delta w / \pi DNt \tag{2}$$

Δw: reduction in weight of the specimen resulting from wear grams (g).

D: diameter of the rotating disc or counterface meters (m).

N: rotational speed or count of revolutions per minute (rpm).

t: overall duration of the test (min).

Table 2. L9 orthogonal array

Exp. No	Particle Size (μm)	Load (N)	Time (min)
1	25	10	10
2	25	15	15
3	25	20	20
4	50	10	15
5	50	15	20
6	50	20	10
7	100	10	20
8	100	15	10
9	100	20	15

2.6 Plan of experiment

The experiments were conducted according to a standard rectangular array protocol. The choice of the orthogonal array was made by making sure the associated degrees of freedom were greater than or equal to the total number of degrees of freedom associated with the wear parameters. In this research, the L9 orthogonal array was chosen for its effectiveness in minimizing the number of experiments while adequately representing the primary effects of three parameters, each at three levels. While the L16 array could provide a more comprehensive analysis of interactions, the L9 was preferred for its equilibrium between experimental expenses and statistical relevance.

It was presumed that the interactions among the parameters were restricted; nevertheless, specific coupled effects between load and particle size were noted and elaborated upon in the results section, as demonstrated in Table 2. The experimental parameters chosen encompass the applied load, duration, and particle size. The design of the experiment comprises nine tests, each aligned with a distinct row in the L9 orthogonal array. The columns of this array signify the various parameter values, with the initial column allocated to particle size, the subsequent column to applied load, and the third to time.

The experiments were executed according to the orthogonal array, with the parameter levels specified in each row of the array. The experimental results were further analyzed using Signal-to-Noise Ratio (SNR). The primary response variable examined was the wear rate, with the aim of minimizing this value. The wear rate was computed employing a logarithmic transformation of the loss function, as detailed below [23].

$$(S/N) = -10 \times \log 1/n \ (\Sigma \ Y_i^2) \tag{3}$$

The variable 'n' represents the number of observations, whereas 'Yi' indicates the documented values for the wear rate and the coefficient of friction. This discussion highlights that the quality characteristics are deemed to have been enhanced when the signal-to-noise (S/N) ratio is reduced.

3. RESULTS AND DISCUSSIONS
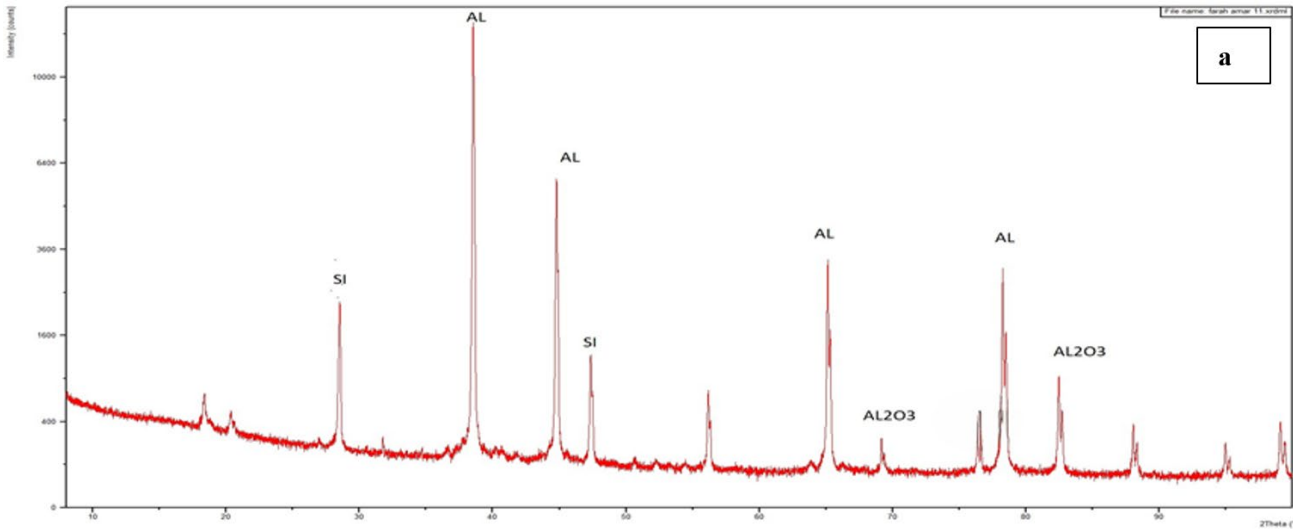
3.1 XRD analysis

The analysis conducted through X-ray diffraction (XRD) demonstrated that the main peaks recognized as Al and SI are indicative of the existence of Al_2O_3 in the alloy, as depicted in the results shown in Figure 1.

Table 3. The intensities (I) and the diffraction angle of the Al-Si alloy containing the additive Al_2O_3 at a particle size of 25 μm

Alloy	Phase	2Theta	I/I1
Al-12%SI	Al	38.40, 44.65, 78.16	100, 48.11, 27.7
Al-12%SI	SI	28.41, 47.24	6.96, 8.27
Al-12%SI	Al_2O_3	69.07, 82.37	1.25, 7.82

Table 4. The intensities (I) and the diffraction angle of the Al-Si alloy containing the additive Al_2O_3 at a particle size of 50 μm

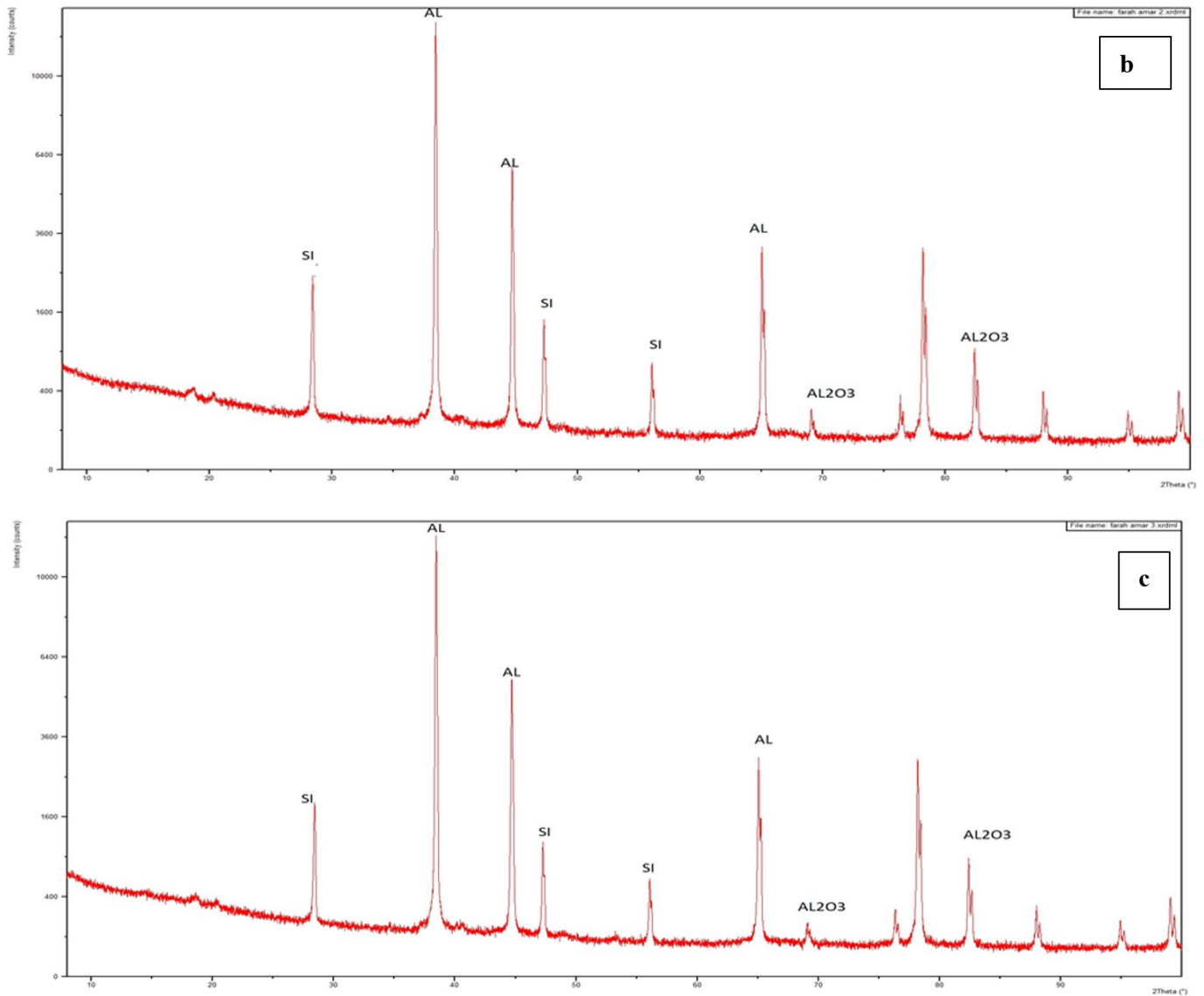| Alloy	Phase	2Theta	I/I1
Al-12%SI	Al	38.41, 44.66, 78.17	100, 47.66, 28.08
Al-12%SI	SI	28.38, 47.25	14.97, 11.15
Al-12%SI	Al_2O_3	69.07, 82.38	1.38, 8.14

Figure 1. XRD analysis of Al-Si14% alloy with adding Al_2O_3

Table 5. The intensities (I) and the diffraction angle of the Al-Si alloy containing the additive Al_2O_3 at a particle size of 100 μm

Alloy	Phase	2Theta	I/I1
Al-12%SI	Al	38.42, 44.67, 78.19	100, 46.10, 28.11
Al-12%SI	SI	28.38, 47.25	12.32, 9.37
Al-12%SI	Al_2O_3	69.08, 82.39	1.03, 7.61

According to Figure 2 and Tables 3-5, distinct diffraction peaks associated with the Al, Si, and Al_2O_3 phases are evident. A gradual decline in the intensity of the Al peaks was observed with the introduction of Al_2O_3 particles, suggesting a potential reduction in crystallinity and the emergence of lattice distortions resulting from the integration of hard ceramic particles into the metallic matrix. Furthermore, the emergence and heightened clarity of peaks near $2\theta \approx 28.4°$ and $69.0°$ validate the development and expansion of Si and Al_2O_3 phases in the reinforced sample.

These alterations in the XRD patterns are intricately linked to the enhancement of mechanical properties. The incorporation of Al_2O_3 particles has led to improved wear resistance and increased hardness, attributed to mechanisms of dispersion strengthening and grain refinement.

3.2 The Scanning Electron Microscope result

The Scanning Electron Microscope has yielded additional insights into the microstructure of the alloy, as evidenced by the results depicted in the test images. The SEM images showcasing the microstructures of the alloys prior to and following the incorporation of Al_2O_3 are displayed in Figure 2.

3.3 The outcome of hardness testing for the Al-Si alloy

The dimensions of Al_2O_3 particles significantly influence the hardness of the composites. In particular, a decrease in the size of the reinforcement particles is associated with an increase in hardness. This is illustrated in Table 6, where composites reinforced with 25 μm Al_2O_3 demonstrate the highest hardness values at 102 HV, compared to those reinforced with 100 μm Al_2O_3, which exhibit the lowest hardness values at 90 HV. Smaller reinforcement particles enhance the contact area with the aluminum matrix, while larger particles lead to a diminished contact area, impeding the diffusion process. Furthermore, Al_2O_3 particles act as barriers to dislocation movement within the aluminum matrix. Each hardness test was performed in triplicate (n = 3), and the mean values were computed. The standard deviation was utilized to

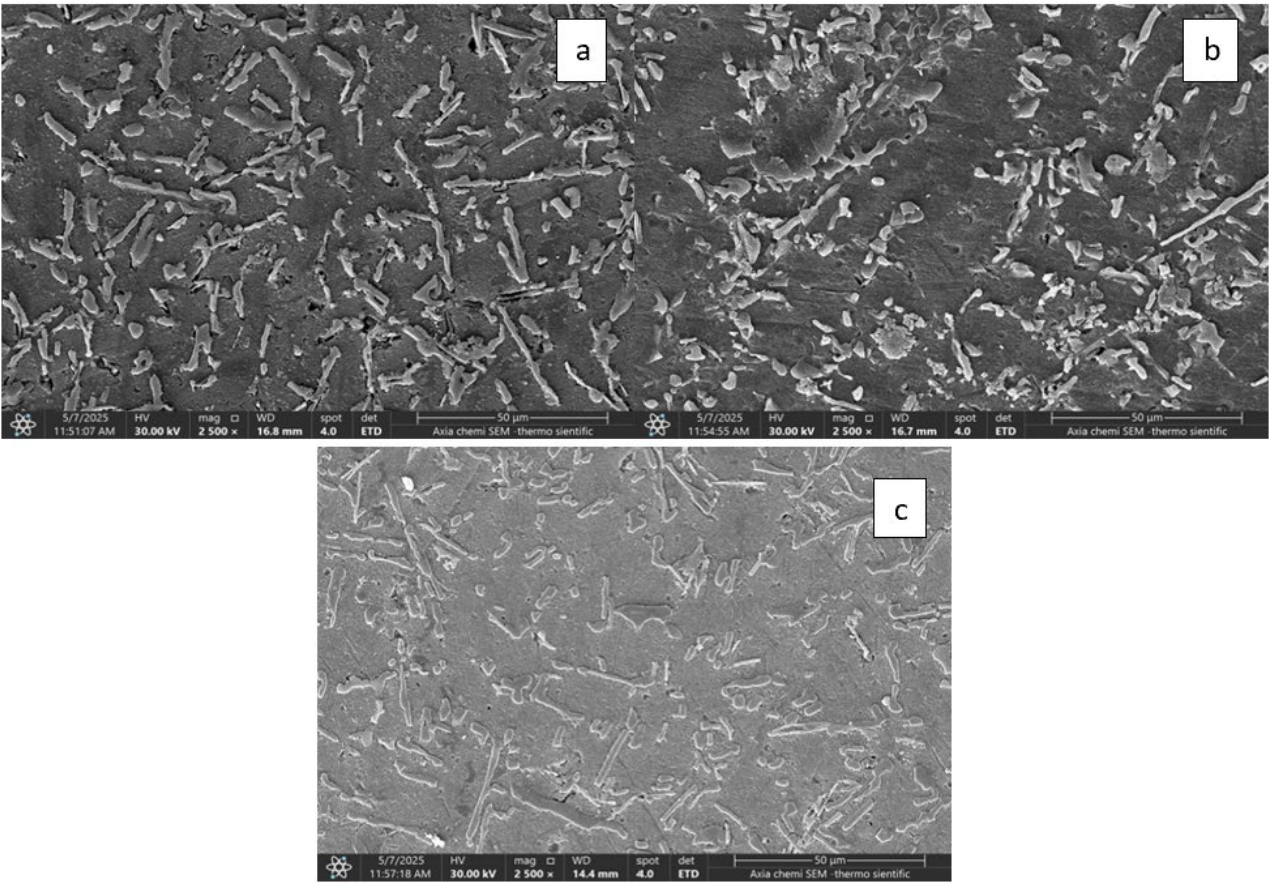indicate the variability of the data. Error bars representing ±1 standard deviation were incorporated in Figure 3.

Figure 2. Scanning Electron Microscope for alloys after addition Al_2O_3, a) Al-12% alloy of Si with additive 25 µm Al_2O_3, b) Al-12% alloy of Si with additive50 µm Al_2O_3, c) Al-12% alloy of Si with additive100 µm Al_2O_3

Table 6. Vickers hardness of the Al-12%Si alloy with Al_2O_3 particle sizes of 25, 50, and 100 µm

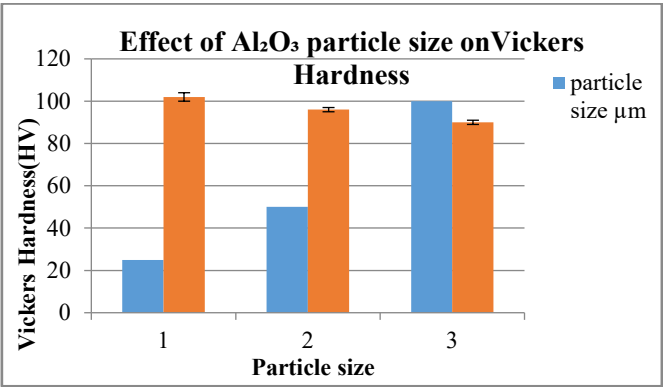| Alloy	Before Addition Al_2O_3	With Addition 25 µm Al_2O_3	With Addition 50 µm Al_2O_3	With Addition 100 µm Al_2O_3
Al-12%Si	80	102	96	90

Figure 3. The relationship between Al_2O_3 particle size and Vickers hardness in fabricated samples

3.4 Result of wear

The research findings and the computed metrics were obtained in alignment with the experimental design. Following this, the results were assessed using the commercial software MINITAB 20.4, which is specifically designed for experimental design and statistical analysis of experimental data. The experimental values related to the wear rate, along with the calculated Signal-to-Noise Ratio (SNR) values for a designated response, as defined by Eq. (3), are presented in Table 7.

3.4.1 Outcomes of the statistical evaluation of the experiments

The research outcomes and computed values were obtained in alignment with the experimental framework, subsequently analyzed using MINITAB 20.4, a commercial software specifically designed for experimental design and statistical evaluation of the experimental setup. The influence of the controlled process parameters on the wear rate is visually represented in Figures 3 and 4. By scrutinizing these results, bolstered by the Signal-to-Noise Ratio (SNR), the optimal conditions leading to the wear rate are depicted in Figures 4 and 5.

3.4.2 Wear rate variance analysis

This analysis aids in recognizing the relative effects of the final parameter on wear rate responses. Table 8 displays the variance analysis, which includes P-values and F-values that demonstrate the impact of each individual parameter on the response characteristics, particularly the arithmetic value of the Signal-to-Noise Ratio (SNR) and the average wear rate.

The P-value presented in Table 8 reflects the extent to which each parameter affects the corresponding response characteristics within the defined range. The results reveal that parameter A is the most critical factor in achieving a minimal wear rate, while parameter B is recognized as the second most significant factor for reducing wear rate, and parameter C ranks third in terms of minimizing wear rate. The statistical results show that particle size (P-value = 0.002) is the most statistically significant factor influencing wear rate. This can be explained by dislocation theory, where finer Al_2O_3 particles act as stronger barriers to dislocation motion, leading to enhanced hardness and wear resistance. Additionally, smaller particles provide a larger surface area for load transfer and better wettability, resulting in improved matrix-particle bonding

3.4.3 Multiple linear regression models

The statistical software MINITAB 20.4 has been utilized to formulate the equation for multiple linear regression. This model delineates the connection between the independent or predictor variable and the response variable by fitting a linear equation to the observed data. The resulting regression equation for the wear rate is as follows (Table 9 and Table 10):

$$W.R*10E\text{-}8 = 4.44444 - 0.21111 \text{ particle size\_25} - 0.01111 \text{ particle size\_50} + 0.22222 \text{ particle size\_100} - 0.12778 \text{ load\_10} - 0.00111 \text{ load\_15} + 0.12889 \text{ Load\_20} - 0.04444 \text{ time\_10} - 0.00444 \text{ time\_15} + 0.04889 \text{ time\_20}$$

Table 7. Orthogonal array (L9) of Taguchi for wear test

Exp. No	Particle Size (µm)	Load (N)	Time (min)	Wear Rate*10E-8 (g/cm)	Predicted of Wear Rate	SN
1	25	10	10	4.05	4.06111	-12.1811
2	25	15	15	4.23	4.22778	-12.5181
3	25	20	20	4.42	4.41111	-12.8852
4	50	10	15	4.31	4.30111	-12.6663
5	50	15	20	4.47	4.48111	-13.0381
6	50	20	10	4.52	4.51778	-13.0941
7	100	10	20	4.59	4.58778	-13.2276
8	100	15	10	4.63	4.62111	-13.2883
9	100	20	15	4.78	4.79111	-13.6205

Table 8. Variance analysis

Source	DF	Adj SS	Adj MS	F	P
Particle size	2	0.282222	0.141111	453.57	0.002
Load	2	0.098822	0.049411	158.82	0.006
Time	2	0.013156	0.006578	21.14	0.045
Error	2	0.000622	0.000311		
Total	8	0.394822		--------------------	------------------
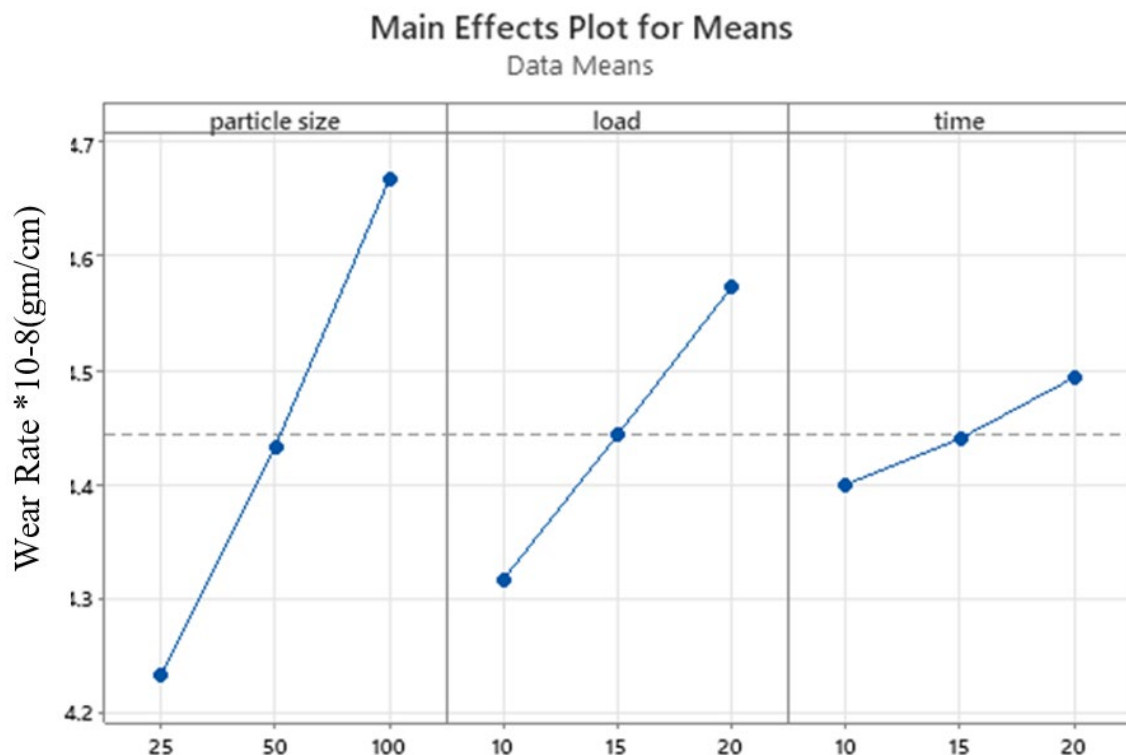
Figure 4. Main effect plot for means for W.R

Main Effects Plot for SN ratios
Data Means

Signal-to-noise: Smaller is better
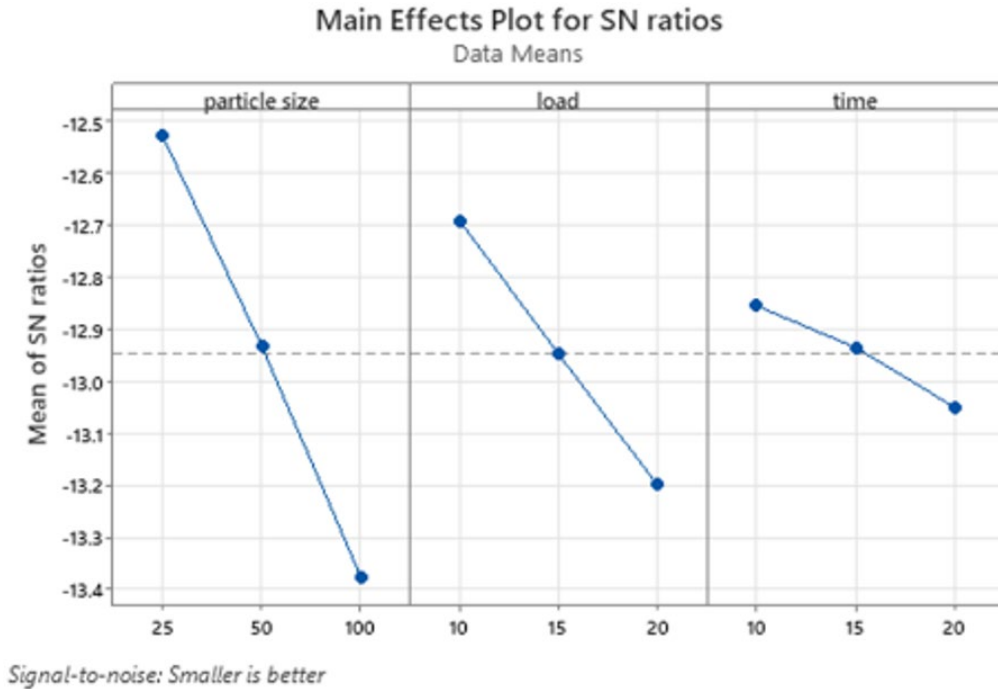
Figure 5. Main effected plot for SN

Table 9. Response table for W.R (Al-12%Si)

Level	Particle Size	Load	Time
1	4.233	4.317	4.400
2	4.433	4.443	4.440
3	4.667	4.573	4.943
Delta	0.433	4.257	0.093
Rank	1	2	3

Table 10. SN ratio smaller is better response for W.R (Al-12%Si)

Level	Particle Size	Load	Time
1	-12.53	-12.69	-12.85
2	-12.93	-12.95	-12.93
3	-13.38	-13.20	-13.05
Delta	0.85	0.51	0.20
Rank	1	2	3

4. CONCLUSIONS

The enhancement of aluminum-silicon alloys through the incorporation of Al_2O_3 particles via the stir casting technique has been effectively executed. The addition of Al_2O_3 markedly increased the hardness of the alloy, rising from 80 HV in the unreinforced variant to 102 HV when utilizing 25 μm particles. An analysis of wear rates, performed using the Taguchi method alongside ANOVA, revealed that particle size was the predominant factor influencing wear, followed by the applied load and the duration of the test. Smaller particles facilitated improved dispersion, enhanced bonding within the matrix, and more efficient resistance to dislocation movement, culminating in superior mechanical properties. In contrast to earlier investigations, this study explores the effects of three different micro-scale sizes of Al_2O_3 particles (25, 50, and 100 μm) and integrates statistical optimization methodologies such as Taguchi analysis, ANOVA, and multiple linear regression modeling. This comprehensive approach enhances the reliability of the results and provides a practical framework for optimizing the performance of composites with minimal experimental effort. The findings indicate promising potential for the developed composites in automotive and aerospace applications where high surface hardness and wear resistance are essential, such as in brake systems and engine components. Furthermore, from a practical perspective, the utilization of micro-sized Al_2O_3 particles is more economically viable and scalable for industrial applications compared to nano-reinforcements. Micro-scale powders are more affordable, simpler to process, and demand less energy during manufacturing. Coupled with the ease and cost-effectiveness of stir casting, the proposed method can be readily implemented in large-scale industrial production with minimal environmental or operational difficulties.

REFERENCES

[1] Singhal, V., Shelly, D., Babbar, A., Lee, S.Y., Park, S.J. (2024). Review of wear and mechanical characteristics of Al-Si alloy matrix composites reinforced with natural minerals. Lubricants, 12(10): 350. https://doi.org/10.3390/lubricants12100350

[2] Badiger, A., Ajay, K.V.S., Sumandas, D. (2016). Wear and mechanical properties assessment of Al-Si/Al_2O_3 nano composites processed by stir casting. International Journal of Research and Innovation in Applied Science (IJRIAS), 1(9): 15-22. https://rsisinternational.org/journals/ijrias/DigitalLibrary/Vol.1&Issue9/15-22.pdf.

[3] Dwivedi, D.K. (2010). Adhesive wear behaviour of cast aluminium–silicon alloys: Overview. Materials & Design (1980-2015), 31(5): 2517-2531.

https://doi.org/10.1016/j.matdes.2009.11.038

[4] Ferrak, A.E.H., Manaa, R., Faiza, K. (2024). Thermomechanical analysis of a gas turbine blade in composite materials with a ceramic (Al_2O_3) coated. Revue des Composites et des Matériaux Avancés-Journal of Composite and Advanced Materials, 34(3): 331-338. https://doi.org/10.18280/rcma.340308

[5] Kumar, V.M., Venkatesh, C.V. (2018). Effect of ceramic reinforcement on mechanical properties of aluminum matrix composites produced by stir casting process. Materials Today: Proceedings, 5(1): 2466-2473. https://doi.org/10.1016/j.matpr.2017.11.027

[6] Ma, P., Jia, Y., Konda Gokuldoss, P., Yu, Z., Yang, S., Zhao, J., Li, C. (2017). Effect of Al_2O_3 nanoparticles as reinforcement on the tensile behavior of Al-12Si composites. Metals, 7(9): 359. https://doi.org/10.3390/met7090359

[7] Chandrashekar, A., Ajaykumar, B.S., Reddappa, H.N. (2018). Mechanical, structural and corrosion behaviour of AlMg4. 5/Nano Al_2O_3 metal matrix composites. Materials Today: Proceedings, 5(1): 2811-2817. https://doi.org/10.1016/j.matpr.2018.01.069

[8] Sajjadi, S.A., Ezatpour, H.R., Beygi, H. (2011). Microstructure and mechanical properties of Al-Al_2O_3 micro and nano composites fabricated by stir casting. Materials Science and Engineering: A, 528(29-30): 8765-8771. https://doi.org/10.1016/j.msea.2011.08.052

[9] Murthy, B.V., Auradi, V., Nagaral, M., Vatnalmath, M., Namdev, N., et al. (2023). Al2014–alumina aerospace composites: Particle size impacts on microstructure, mechanical, fractography, and wear characteristics. ACS Omega, 8(14): 13444-13455. https://doi.org/10.1021/acsomega.3c01163

[10] Abbas, I.A., Al-Mayalee, K.H. (2024). Structural and optical properties of Al_2O_3 nanostructures prepared by hot water treatment method. Revue des Composites et des Matériaux Avancés-Journal of Composite and Advanced Material, 34(4): 527-532. https://doi.org/10.18280/rcma.340414

[11] Kang, N., Coddet, P., Liao, H., Baur, T., Coddet, C. (2016). Wear behavior and microstructure of hypereutectic Al-Si alloys prepared by selective laser melting. Applied Surface Science, 378: 142-149. https://doi.org/10.1016/j.apsusc.2016.03.221

[12] Mishra, D., Nanda, A.K. (2023). Experimental investigation on mechanical properties of stir casted aluminum SiC metal matrix composites. Materials Today: Proceedings, 74: 1023-1027. https://doi.org/10.1016/j.matpr.2022.11.412

[13] Krishna, V., Shankar, V.K., Muniyappa, L.M., Benal, M.M. (2020). Prediction of temperature during machinability of Al_2O_3 reinforced Al7075. Revue des Composites et des Matériaux Avancés-Journal of Composite and Advanced Materials, 30(5-6): 241-246. https://doi.org/10.18280/rcma.305-607

[14] Kumar, A., Singh, R.C., Chaudhary, R. (2020). Recent progress in production of metal matrix composites by stir casting process: An overview. Materials Today: Proceedings, 21: 1453-1457. https://doi.org/10.1016/j.matpr.2019.10.079

[15] Labus Zlatanovic, D., Pierre Bergmann, J., Balos, S., Hildebrand, J., Bojanic-Sejat, M., Goel, S. (2023). Effect of surface oxide layers in solid-state welding of aluminium alloys–Review. Science and Technology of Welding and Joining, 28(5): 331-351. https://doi.org/10.1080/13621718.2023.2165603

[16] Dwivedi, S.P., Srivastava, A.K., Maurya, N.K., Maurya, M. (2019). Microstructure and mechanical properties of Al 6061/Al_2O_3/Fly-Ash composite fabricated through stir casting. Annales de Chimie: Science des Materiaux, 43(5): 341-348. https://doi.org/10.18280/acsm.430510

[17] Mussatto, A., Ahad, I.U., Mousavian, R.T., Delaure, Y., Brabazon, D. (2021). Advanced production routes for metal matrix composites. Engineering Reports, 3(5): e12330. https://doi.org/10.1002/eng2.12330

[18] Gharaibeh, N., AlAjlouni, M., Rayes, A. (2024). Structural and mechanical characterization of aluminum matrix nanocomposites reinforced with SiC and Al_2O_3 nanoparticles. Revue des Composites et des Matériaux Avancés-Journal of Composite and Advanced Material, 34(6): 749-754. https://doi.org/10.18280/rcma.340609

[19] Zykova, A., Martyushev, N., Skeeba, V., Zadkov, D., Kuzkin, A. (2019). Influence of W addition on microstructure and mechanical properties of Al-12%Si alloys. Materials, 12(6): 981. https://doi.org/10.3390/ma12060981

[20] Ali, K.G., Taieh, N.K., Khudhur, S.K. (2022). Investigation of dry tribo-behavior of aluminum alloy AA6061/Al_2O_3/graphite composites synthesized by stir casting technique. Revue des Composites et des Matériaux Avancés-Journal of Composite and Advanced Materials, 32(5): 253-259. https://doi.org/10.18280/rcma.320506

[21] El Garchani, F.E., Lgaz, H., Kaya, S., Lee, H.S., Ibrahim, S.M., et al. (2023). Effects of heat treatment on the corrosion behavior and mechanical properties of aluminum alloy 2024. Journal of Materials Research and Technology, 25: 1355-1363. https://doi.org/10.1016/j.jmrt.2023.05.278

[22] Rumi, M.J.U., Rahman, M.M. (2023). Characterization on specific wear rate of Al composite reinforced with nano-Al_2O_3 using Taguchi's technique. Tribologia-Finnish Journal of Tribology, 40(1-2): 37-45. https://doi.org/10.30678/fjt.125959

[23] Abed, S.A., Hassan, S.R., Jomah, A.J.S., Hanon, M.M. (2023). Prediction on the wear rate of epoxy composites reinforced micro-filler of the natural material residue using Taguchi–neural network. EUREKA: Physics and Engineering, 6: 149-159.